Simulation of the Cyclic Response of Anisotropic Clay through Bounding Surface Viscoplasticity

Mohammad Zarrabi,[1] Zhenhao Shi,[2] & Samuel Yniesta,[3]

[1]PhD Candidate, Department of Civil, Geological and Mining Engineering, Polytechnique Montréal, Montreal, Canada;
[2]Key Laboratory of Geotechnical and Underground Engineering of Ministry of Education, Tongji University, Shanghai, China;
[3]Assistant Professor, Department of Civil, Geological and Mining Engineering, Polytechnique Montréal, Montreal, Canada;
Giuseppe Buscarnera[4]
[4]Associate Professor, Department of Civil and Environmental Engineering, Northwestern University, Evanston, IL, US;

ABSTRACT
In this study, a recently developed framework referred to as bounding surface elasto-viscoplasticity (BS-EVP) is used to combine bounding surface concepts and the Perzyna's overstress theory, thus enabling the simulation of rate effects for general degrees of overconsolidation. At variance with previous analyses, the model proposed here suppresses the hypothesis of isotropy and enables the simulation of fabric effects through rotational hardening. For this purpose, the SANICLAY model is recast in light of the BS-EVP framework by enabling the growth of the overstress and the consequent accumulation of viscous strain within the bounding surface. It is shown that the resulting constitutive model captures the dependence of the undrained strength of clays on the loading rates. Additionally, by employing a proper repositioning of the projection center and a hybrid flow rule, the performance of the model is improved to make it a robust model for cyclic loading applications and cyclic softening analysis.

RÉSUMÉ
Dans cette étude, le concept récemment développé appelé élasto-viscoplasticité à surface limitante (BS-EVP) est utilisé pour combiner les concepts de surface limitante et la théorie de contraintes excessives de Perzyna, permettant ainsi la modélisation des effets de taux de déformation pour différents degrés de surconsolidation. Contrairement aux analyses précédentes, le modèle proposé ici supprime l'hypothèse d'isotropie et permet de simuler les effets de structure par écrouissage rotationnel. Dans ce but, le modèle SANICLAY est refurmulé avec le concept de BS-EVP en permettant la croissance de contraintes excessives et l'accumulation conséquente de déformation visqueuse dans la surface limite. Il est montré que la loi de comportement résultant saisit la dépendance de la résistance non drainée des argiles sur les taux de chargement. De plus, en utilisant un repositionnement approprié du centre de projection et une règle d'écoulement plastique hybride, les performances du modèle sont améliorées pour en faire un modèle robuste pour les applications de chargement cyclique et l'analyse de ramollissement cyclique.

1 INTRODUCTION

Liquefaction induced by a seismic event is defined as the loss of strength of loose saturated granular soils under cyclic loading (Jefferies and Been, 2015). Liquefaction can considerably damage manmade and natural earth structures and cause loss of human properties and lives, as has been reported in many major earthquakes (such as the 1964 Niigata earthquake (Seed and Idriss, 1971) and the 2011 Christchurch earthquake (Bradley and Cubrinovsky, 2011) to name a few).

Clay-like materials can also exhibit a severe strength loss associated with large plastic deformations in the course of an earthquake. Evidence of such strength loss in clays, which is referred to as cyclic softening (Boulanger and Idriss, 2006), has been reported in a few case histories (such as the fourth avenue landslide during the 1964 Alaskan earthquake (Stark and Contreras, 1998), the 1999

Chi-Chi earthquake in Taiwan (Shou and Wang, 2003), and the Carrefour Shopping Center case history from the 1999 Kocaeli earthquake (Martin et al., 2004)).

Numerical simulations may be used as a mean to analyze the potential consequences of liquefaction and cyclic softening. In this regard, several constitutive models have been developed so far, most of which within the critical state framework. However, despite a significant amount of work on the constitutive modeling of liquefiable soils (e.g. Dafalias and Manzari ,2004, UBCSAND (Beaty and Byrne, 2011), PM4SAND (Boulanger and Ziotopoulou, 2017)), much less attention has been given to the modeling of cyclic softening in clay, partially because only a few case studies of earthquake-induced ground failure in claylike soils have been reported (Chu et al., 2008).

Recently two bounding surface plasticity models for cyclic softening have been developed by Seidalinov and Taiebat (2014) and Shi et al. (2018) upon the framework of the SANICLAY family model (Dafalias et al. 2006; Taiebat et al. 2010). Although these constitutive laws are valuable tools to study cyclic loading, neither considers the effect of loading rate and/or soil viscosity in their formulation.

To include rate and time effects into bounding surface plasticity, an elasto-viscoplastic framework was proposed by Shi et al. (2019) by combining the Perzyna's overstress theory with the bounding surface plasticity. While any baseline bounding surface model could be used for such extension, for simplicity, the first application was based on the modified Cam-Clay (Roscoe and Burland, 1968).

In this study, the bounding surface elasto-viscoplasticity framework (BS-EVP) is used in the context of the SANICLAY model (Dafalias et al. 2006), thus using a rotational hardening rule, a procedure for the relocation of the projection center, and a hybrid flow rule. It will be shown that such reformulation enables the description of anisotropic properties and higher fidelity in replicating the cyclic loading response of clays, including pore water pressure built-up, hysteresis loops, and effective stress path at different loading rates and/or frequencies.

2 MODEL FORMULATION IN TRIAXIAL SPACE

To facilitate the formulation, this section describes the key components of the constitutive model with reference to the triaxial space. As a result, the model functions are given in terms of the mean effective stress p, deviatoric stress, q, volumetric strain, ε_v, and deviatoric strain, ε_q, defined as:

$$p = \frac{\sigma_a + 2\sigma_r}{3} \quad [1]$$

$$q = \sigma_a - \sigma_r \quad [2]$$

$$\varepsilon_v = \varepsilon_a + 2\varepsilon_r \quad [3]$$

$$\varepsilon_q = \frac{2}{3}(\varepsilon_a - \varepsilon_r) \quad [4]$$

Where σ_a and σ_r are axial and radial stresses, respectively and ε_a and ε_r are axial and radial strains, respectively.

2.1 Elastic response

According to Perzyna's theory of viscoplasticity, the total strain rate is additively decomposed into an elastic part and a viscoplastic part:

$$\dot{\varepsilon} = \dot{\varepsilon}^e + \dot{\varepsilon}^{vp} \quad [5]$$

Where the superposed dot denotes a rate and superscripts e and vp stand for elastic and viscoplastic, respectively. The components of the elastic strain rate are commonly expressed based on an isotropic hypoplastic law:

$$\dot{\varepsilon}_v^e = \frac{\dot{p}}{K} \quad [6]$$

$$\dot{\varepsilon}_q^e = \frac{\dot{q}}{3G} \quad [7]$$

Where subscripts v and q stand for the volumetric and deviatoric strains, respectively. Also, K and G are the bulk and shear moduli, respectively, which are expressed as:

$$K = \frac{(1+e)p}{\kappa} \quad [8]$$

$$G = \frac{3(1-2v)}{2(1+v)}K \quad [9]$$

Where v and e are the Poisson's and void ratios, respectively, and κ is the slope of isotropic unloading in the e-ln(p) plot.

2.2 Bounding and viscoplastic potential surfaces

To account for soil anisotropy, the yield surface of the SANICLAY model proposed by Dafalias et al. (2006) uses a distorted and rotated ellipse. In this study, this particular yield surface shape is used for the bounding surface, as previously done by Seidalinov and Taiebat (2014) and Shi et al. (2016). This bounding surface is schematically shown in Figure 1 and expressed as:

$$F = (\bar{q} - \bar{p}\alpha)^2 - (N^2 - \alpha^2)\bar{p}(p_0 - \bar{p}) = 0 \quad [10]$$

Where $(\bar{p}, \bar{q})$ is the image stress point obtained by mapping the current stress (p, q) on the bounding surface from a projection center $PC\ (p_c, q_c)$ through a mapping rule which will be detailed in the following sections. α and p_0 are rotational and isotropic hardening variables representing anisotropic states and soil consolidation, respectively, and N is a parameter controlling the distortion of the bounding surface.

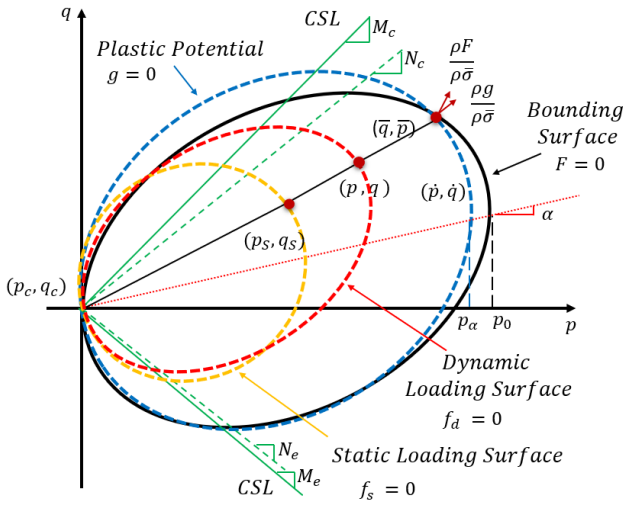

Figure 1. Schematic of bounding surface, plastic potential surface, and static loading surface of the BS-EVP model.

In the rate-independent bounding surface plasticity, the image stress lies on the bounding surface, whereas the current stress lies on the implicitly defined loading surface. Extending the Perzyna's theory of viscoplasticity (Perzyna, 1963) to a bounding surface framework requires the use of two distinct surfaces functional to compute the evolution of a modified overstress. Hereafter, such surfaces are defined as *static* and *dynamic* loading surfaces, which replace the role of the loading surface of rate-independent bounding surface models (Shi et al., 2019). As shown in Figure. 1, the static and dynamic loading surfaces are the locus of the static (p_s, q_s) and current stress (p, q), respectively. Use of the Perzyna's overstress concept implies that the state of stress can lay inside, on, or outside the static loading surface. However, the stress state inside the static loading surface can only cause elastic deformation, while states of stress outside it causes viscoplastic strain with a magnitude dependent on the degree of violation of the static loading surface (here referred to as overstress).

The model uses a non-associated flow rule, therefore requiring the definition of a flow potential surface different than the bounding surface to calculate the viscoplastic strain:

$$g = (\bar{q} - \bar{p}\alpha)^2 - (M^2 - \alpha^2)\bar{p}(p_\alpha - \bar{p}) = 0 \qquad [11]$$

Where M is the slope of the critical state line in the $p - q$ space, and p_α is the value of $\bar{p}$ at $\bar{q} = \alpha\bar{p}$ to adjust the plastic potential for a given pair of the image stress on the bounding surface.

2.3 Image stress and projection center

The key idea of bounding surface plasticity is that the current stress is related to a corresponding counterpart stress state on the bounding surface through a specifically defined mapping rule. A usual choice is a radial mapping rule, which, similar to earlier propositions by Dafalias and Herrmann (1986), can be expressed as:

$$\bar{p} = p_c + b_d(p - p_c) \qquad [12]$$

$$\bar{q} = q_c + b_d(q - q_c) \qquad [13]$$

Where $1 \leq b_d \leq \infty$ indicates the similarity ratio between the dynamic loading surface and the bounding surface, respectively, and the two extremes correspond to a current stress coinciding with the image stress ($b_d = 1$) or the projection center ($b_d = \infty$). Along the same lines, given the relation of both static and current stress to the same image stress, it is possible to define a similarity ratio b_s also for the static loading surface. Knowledge of both b_s and b_d, allows the static stress to be expressed as a function of the current stress, as follows:

$$p_s = p_c + \frac{b_d}{b_s}(p - p_c) \qquad [14]$$

$$q_s = q_c + \frac{b_d}{b_s}(q - q_c) \qquad [15]$$

Contrary to the dynamic loading surface, the static loading surface moves according to its own evolution law, encapsulated in the rate of b_s. Such viscoplastic hardening rule will be discussed in the following section.

In order to have a unique image stress, the projection center should always be located inside the bounding surface. Seidalinov (2012) and Seidalinov and Taiebat (2014) suggested that updating the projection center at any stress reversal improves the predictive capability of the model for the cyclic response of clays. It can be shown that the stress reversal occurs whenever the loading index $L \leq 0$, where L can be obtained by satisfying the consistency condition, $\dot{F} = 0$:

$$L = \frac{\frac{\partial g}{\partial \bar{p}}\dot{p} + \frac{\partial g}{\partial \bar{q}}\dot{q}}{K_p} \qquad [16]$$

Where K_p is the plastic modulus, to be defined later. If the projection center is unchanged till the next stress reversal, it might be located outside the bounding surface as the latter shrinks, expands, and/or rotates. Therefore, Seidalinov (2012) and Seidalinov and Taiebat (2014) proposed using a moving projection center to ensure that it always remains inside the bounding surface. In the current study, the evolution rule for the projection center proposed by Shi et al. (2018) is used in which the simultaneous changes of p_0 and α are considered:

$$\dot{p_c} = \frac{p_c}{p_0}\dot{p_0} \quad [17]$$

$$\dot{q_c} = \frac{q_c}{p_0}\dot{p_0} + \frac{N^2 p_c - \alpha q_c}{N^2 - \alpha^2}\dot{\alpha} \quad [18]$$

2.4 The viscoplastic hybrid flow rule

In Perzyna's theory of Viscoplasticity, the viscoplastic strain rates are given as:

$$\dot{\varepsilon}_v^p = \mu\langle\phi(y)\rangle R_v \quad [19]$$

$$\dot{\varepsilon}_d^p = \mu\langle\phi(y)\rangle R_d \quad [20]$$

Where μ is the fluidity parameter, R_v and R_d are the volumetric and deviatoric gradients of the flow potential function, g, respectively, and $\phi(y)$ is the overstress function. The latter is a normalized measure of the distance between the dynamic loading surface and the static loading surface. The use of Macauley brackets ensures that for stress states inside the elastic nucleus, y, the overstress function, $\phi(y)$, yields zero, resulting in no viscoplastic strain development:

$$\langle\phi(y)\rangle = \begin{cases}\phi(y) & if \quad y > 0\\ 0 & if \quad y \le 0\end{cases} \quad [21]$$

Numerous overstress functions have been proposed in the literature (Kaliakin and Dafalias (1990); Martindale et al. (2013); Yin and Hicher (2008)). Here, an exponential form is adopted:

$$\phi = \mu_1 \cdot e^{\mu_2\left(\langle\frac{b_s}{b_d} - 1\rangle\right)} \quad [22]$$

In the following it will be shown that the use of two distinct viscous parameters μ_1 and μ_2 in the overstress function leads to a more versatile viscoplastic formulation and an improved performance in capturing rate effects.

To find R_v and R_d, Seidalinov and Taiebat (2014) used the volumetric and deviatoric gradients of the plastic potential surface at the image stress as the flow rule of the rate-independent bounding surface model (i.e. $R_v = R_v^i$ and $R_d = R_d^i$). The main limitation of that flow rule, hereafter referred to as image stress flow rule, was the occurrence of the effective stress path lock-up after a few cycles of loading in an undrained cyclic loading test. Shi et al. (2016) have shown that employing a hybrid flow rule, i.e. using the gradients of the plastic potential at both image and current stress, may improve such stress path lock-up and add a so-called butterfly-shaped loop to the stress path of the model. In this work, the hybrid flow rule proposed by Shi et al. (2016) is applied for R_v while R_d is solely determined by the image stress flow rule:

$$R_v = R_v^i g_i + R_v^c (m_g - g_i) \quad [23]$$

$$R_d = R_d^i \quad [24]$$

Where m_g is a hybrid flow rule input parameter and g_i is the distribution variable. R_v^i and R_v^c are volumetric gradients of the viscoplastic potential surface at the image and current stress, respectively, and R_d^i is the deviatoric gradient of it at the image stress (refer to Figure. 1). It should be highlighted that the hybrid flow rule in this model is non-associative as the model uses two plastic potential surfaces other than a bounding surface. g_i is assumed to have the following expression:

$$g_i = \left(\frac{1}{b_s}\right)^{\omega} \quad [25]$$

Where ω is a material constant that along with m_g controls the contribution of R_v^c and R_v^c to the flow rule. It should be noted that the special case of $\omega = 0$ and $m_g = 1$ will result in an image stress flow rule. Consequently, R_v^i, R_v^c, and R_d^i are given as:

$$R_v^i = \frac{\partial g}{\partial \bar{p}} = \bar{p}(M^2 - \bar{\eta}^2) \quad [26]$$

$$R_d^i = \frac{\partial g}{\partial \bar{q}} = 2\bar{p}(\bar{\eta} - \alpha) \quad [27]$$

$$R_v^c = p(M^2 - s_l\eta^2) \quad [28]$$

Where η and $\bar{\eta}$ are the current ($\eta = \frac{q}{p}$) and image stress ratio ($\bar{\eta} = \frac{\bar{q}}{\bar{p}}$), respectively, and s_l is a variable that

alternates between 1 and -1 depending on the loading direction.

2.5 The relocation of the static loading surface

As mentioned previously, in Perzyna's viscoplasticity, any stress state inside the static loading surface will result in an elastic response. Therefore, in a monotonic loading, once the stress state exits the static loading surface, the viscoplastic deformations start and continue to develop until the end of the loading. However, in a cyclic loading event when the stress reversal brings the stress state back inside the static loading surface, viscoplastic deformations stop until the stress state is beyond the static loading surface again. Since such abrupt changes of response after stress reversal do not occur in rate-independent bounding surface models, Shi et al. (2019) proposed to eliminate this inconvenience by relocating the static loading surface once two conditions occur simultaneously: (1) current stress is inside the static loading surface and (2) the loading index attains a positive value. These conditions can be expressed as:

$$b_s = b_d \quad if\ (L > 0\ \ and\ \frac{b_s}{b_d} < 1\ ) \tag{29}$$

This relocation procedure mitigates the lack of visco-plastic effects upon stress reversal, in that it promotes the overstress growth as a result of a positive incremental loading index.

2.6 Hardening variables

To complete all parts of the viscoplastic model, it is necessary to express the evolution laws for the hardening variables p_0, α, and b_s. The evolution law of p_0 coincides with that of classical critical state soil mechanics models:

$$\dot{p_0} = \langle \phi(y) \rangle \bar{p}_0 = \langle \phi(y) \rangle \left(\frac{1+e}{\lambda - \kappa}\right) \bar{p}_0 (R_v) \tag{30}$$

For α, the rotational hardening rule proposed by Dafalias et al. (2006) is used:

$$\dot{\alpha} = \langle \phi(y) \rangle \bar{\alpha} \tag{31}$$

$$\bar{\alpha} = \langle \phi(y) \rangle \left(\frac{1+e}{\lambda - \kappa}\right) C \left(\frac{\bar{p}}{p_0}\right)^2 |R_v||\bar{\eta} - x\alpha|(\alpha^b - \alpha) \tag{32}$$

Where λ and κ are the slopes of the isotropic loading and reloading curves in the $p - \ln(e)$ space, respectively, and C and x are input parameters governing the rotational rate of change of the bounding surface and the upper bound of α in a constant stress ratio loading, respectively. Also, α^b is the bounding value for α.

As mentioned previously, the static loading surface has its own evolution law:

$$\dot{b_s} = \langle \phi(y) \rangle \bar{b}_s \tag{33}$$

As suggested by Shi et al. (2018), $\dot{b_s}$ can be inferred from the consistency condition of the underlying rate-independent model used to construct the viscoplastic formulation:

$$\bar{b}_s = \frac{\left(-b_s K_p + \bar{K}_p - (1 - b_s)\left(\frac{\partial F}{\partial \bar{p}}\bar{p}_c + \frac{\partial F}{\partial \bar{q}}\bar{q}_c\right)\right)}{(p - \bar{p}_c)\left(\frac{\partial F}{\partial \bar{p}}\right) + (q - \bar{q}_c)\left(\frac{\partial F}{\partial \bar{q}}\right)} \tag{34}$$

Where K_p and $\bar{K}_p$ are the plastic modulus at the current and image stresses, respectively.

2.7 Plastic modulus and damage variable

The core feature of the bounding surface framework is that the plastic modulus at the current stress, K_p, is associated with the plastic modulus, $\bar{K}_p$, at the image stress allowing permanent strain to occur even if the stress state does not lie on the bounding surface. In this work, the expression of K_p proposed by Shi et al. (2018) is adopted:

$$K_p = \bar{K}_p + (b_s - 1)(1 + e)hp_0^3 \tag{35}$$

Where h is a shape hardening variable that controls the shape of the plastic modulus. Here, a decaying expression for h is used, in agreement with earlier propositions by Seidalinov and Taiebat (2014), who showed that to prevent hysteresis loop lock-up h should not be constant. As a result, the following expression is adopted:

$$h = \frac{h_0}{1 + d} \tag{36}$$

Where h_0 is the initial value of h and d is the damage state variable, the rate of change of which is assumed to be linearly proportional to the deviatoric plastic strain increment:

$$\dot{d} = a_d \left|\dot{\varepsilon}_d^p\right| \tag{37}$$

Finally, $\bar{K}_p$ is obtained by satisfying the consistency condition, $\dot{F} = 0$:

$$\bar{K}_p = -\left(\frac{\partial F}{\partial p_0}\bar{p}_0 + \frac{\partial F}{\partial \alpha}\bar{\alpha}\right) \quad [38]$$

3 RESULTS AND DISCUSSIONS

In this section, the performance of the model in simulating soil response under different loading conditions is discussed. The initial values for the model state variables are summarized in Table 1. Also, the model input parameters are summarized in Table 2.

The performance of the model in simulating an undrained monotonic triaxial loading at four different OCR values of 1, 2, 4, 8, and two axial loading rates of 1%/h and 10%/h is shown in Figure 2. This figure shows that applying the SANICLAY bounding surface allows the model to consider the effect of consolidation history on the undrained monotonic loading. Also, as expected, as the axial loading strain rate increases so does the monotonic strength. It should be mentioned that for these simulations, the use of an exponential-type overstress function and assigning low values for viscosity parameters (μ_1 and μ_2) have caused the increase of the soil strength with the loading rate to be subtle. However, if desired, employing another types of overstress functions along with assigning other values for viscous parameters will change the effect of axial loading rates on the increase of the monotonic strength.

Table 1. Initial conditions

Category	Parameter	Value
Initial void ratio	e	0.7
Initial size of the bounding surface (kPa)	p_0	200
Initial orientation of the bounding surface	α	0
Initial value of the static similarity ratio	b_s	1

Table 1. Model input parameters

Category	Input Parameter	Value
Elasticity	κ	0.03
	ν	0.2
Critical state	λ	0.15
	M	1
Bounding surface	N	1
Plastic modulus	h_0	100
	a_d	100
Rotational hardening	C	5
	x	1.7
Hybrid flow rule	ω	5
	m_g	0.3
Viscosity	μ_1	1e-8
	μ_2	50

As can be seen in these figures, due to the use of the bounding surface concept with a proper relocation of the projection center, a large elastic response, which is typical of the MCC, does not occur in the mean effective stress path, indicating that the plastic response occurs at the very initiation of the cyclic loading. Additionally, the use of a hybrid flow rule improves the mean effective stress path response by enabling the simulation of so-called butterfly loops. Finally, as the loading frequency increases, the accumulated deviatoric strain and the pore water pressure reduces. Such rate-dependent behavior is consistent with what has been reported in different studies (Li et al., 2011; Ni et al., 2014).

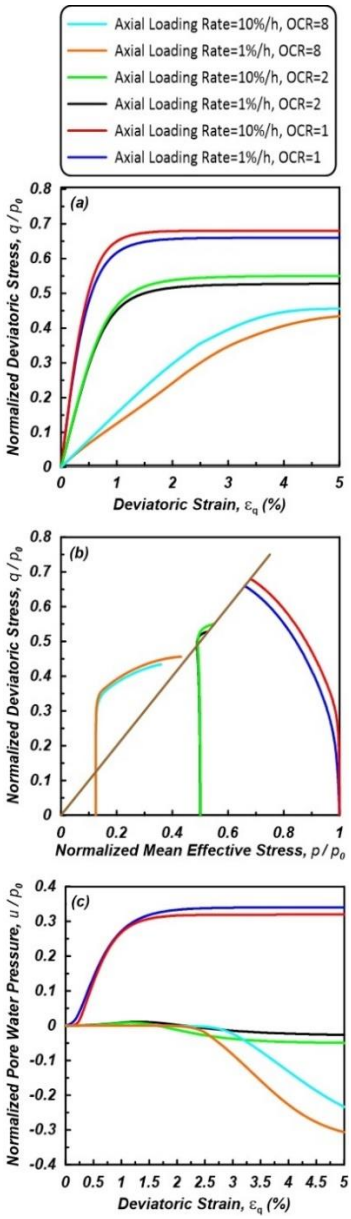

Figure 2. Undrained monotonic triaxial compression tests simulated by the BS-EVP model at different OCRs and loading rates.

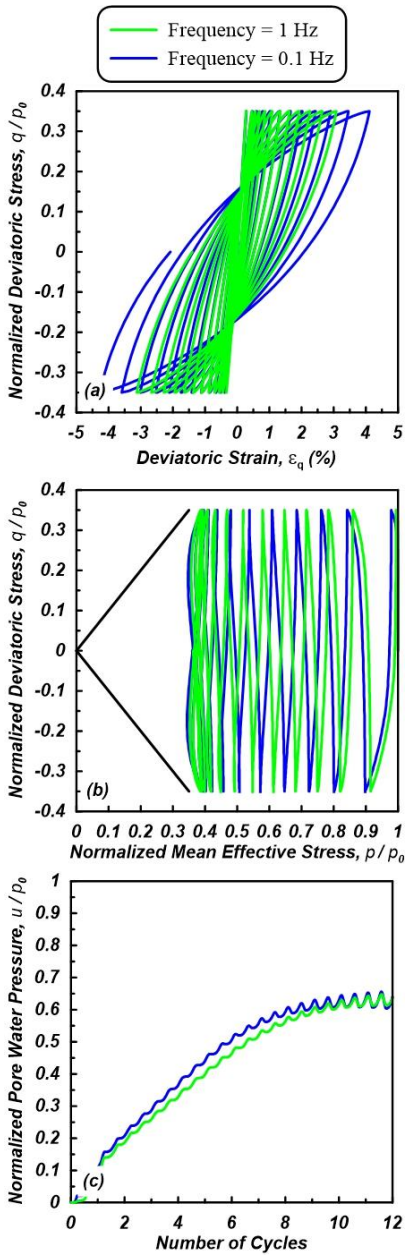

Figure 3. Effective stress path and the hysteresis loops of stress-controlled undrained cyclic triaxial tests simulated by the BSVP model.

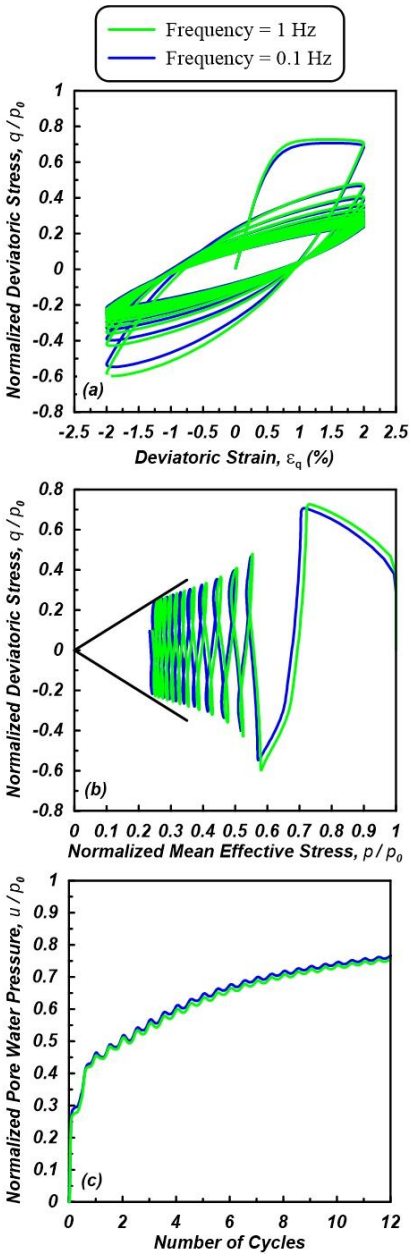

Figure 4. Effective stress path and the hysteresis loops of strain-controlled undrained cyclic triaxial tests simulated by the BSVP model.

4 SUMMARY AND CONCLUSIONS

In this study, the SANICLAY model was reformulated in a rate-dependent form by using the bounding surface elasto-viscoplasticity framework proposed by Shi et al. (2019). Such reformulation was based on a rotational hardening rule, a proper projection center update, and a hybrid flow rule. It was shown that the resulting model is characterized by improved capabilities in replicating the cyclic response of anisotropic clay at varying loading rates. In particular, it was shown that the model captures changes in undrained strength caused by different monotonic loading rates, as well as changes in pore pressure build up resulting from changes in cyclic loading frequency, thus enabling more robust cyclic softening simulations.

In addition to the above features, it was shown that the use of an overstress viscoplastic formulation in a bounding surface context enables the simulation of rate effects for clays characterized by different degrees of consolidation. Most importantly, these features were shown to lead to a realistic prediction of time-dependent pore water pressure generation and strain accumulation.

Future works will involve the discussion of the model input parameters, implementation of the proposed elasto-viscoplastic model into a numerical modeling software, and

its validation against laboratory and field data to further assess its ability to solve geotechnical problems characterized by both monotonic and cyclic loading.

5 ACKNOWLEDGEMENT

Funding from the National Science and Engineering Research Council (NSERC) of Canada and Mitacs Globalink Research Award is gratefully acknowledged. Any opinions, findings, conclusions, or recommendations expressed in this material are those of the author(s) and do not necessarily reflect the views of the funding agencies.

6 REFERENCES

Bradley, B. A. and Cubrinovski, M. 2011. Near-source strong ground motions observed in the 22 February 2011 Christchurch earthquake, Seismological Research Letters, 82(6): 853-865.

Boulanger, R. W. and Idriss, I. M. 2006. Liquefaction susceptibility criteria for silts and clays, Journal of geotechnical and geoenvironmental engineering, 132(11): 1413-1426.

Boulanger, R. W. and Ziotopoulou, K. 2017. PM4Sand (version 3.1): A sand plasticity model for earthquake engineering applications. Report No. UCD/CGM-17/01, Center for Geotechnical Modeling, Department of Civil and Environmental Engineering, University of California, Davis, CA, March, 114 pp.

Beaty, M. H. and Byrne, P. M. 2011. UBCSAND constitutive model version 904aR. Itasca UDM Web Site, 69.

Chu, D. B. Stewart, J. P. Boulanger, R. W. and Lin, P. S. 2008. Cyclic softening of low-plasticity clay and its effect on seismic foundation performance. *Journal of geotechnical and geoenvironmental engineering*, ASCE, 134(11), 1595-1608.

Dafalias, Y. F. and Herrmann, L. R. 1986. Bounding surface plasticity. II: application to isotropic cohesive soils. *Journal of Engineering Mechanics,* ASCE, 112(12): 1263–1291.

Dafalias Y. F. and Manzari, M. T. 2004. Simple plasticity sand model accounting for fabric change effects. Journal of Engineering Mechanics, 130(6): 622–634.

Dafalias, Y. F. Manzari, M. T. and Papadimitriou, A. G. 2006. SANICLAY: simple anisotropic clay plasticity model. *International Journal for Numerical and Analytical Methods in Geomechanics*, 30(12): 1231-1257.

Dafalias, Y. F. Taiebat, M. 2013. Anatomy of rotational hardening in clay plasticity, *Géotechnique,*63(16):1406.

Dafalias, Y. F. Taiebat, M. 2014. Rotational hardening with and without anisotropic fabric at critical state. *Géotechnique,* 64(6): 507–11

Perzyna, P. 1963. The constitutive equations for rate sensitive plastic materials. *Quarterly of Applied Mathematics*, 20(4): 321–332.

Seed, H. B. and Idriss, I. M. 1971. Simplified procedure for evaluating soil liquefaction potential, Journal of Geotechnical Engineering, ASCE, 97(9): 1249–1273.

Seidalinov, G. 2012. A simple anisotropic bounding surface plasticity model for cyclic response of clays. M.A.Sc. thesis, University of British Columbia, Vancouver, British Columbia, Canada, 2012.

Seidalinov, G. and Taiebat, M. 2014. Bounding surface SANICLAY plasticity model for cyclic clay behavior. *International Journal for Numerical and Analytical Methods in Geomechanics*, 38(7): 702-724.

Shou, K. J. and Wang, C. F. 2003. Analysis of the Chiufengershan landslide triggered by the 1999 Chi-Chi earthquake in Taiwan, *Engineering Geology*, 68(3-4), 237-250.

Stark, T. D. and Contreras, I. A. 1998. Fourth Avenue landslide during 1964 Alaskan earthquake, Journal of Geotechnical and Geoenvironmental Engineering, 124(2): 99-109.

Jefferies, M. and Been, K. 2015. Soil liquefaction: a critical state approach, CRC press.

Kaliakin, V. N. Dafalias, Y. F. 1990. Theoretical aspects of the elastoplastic-viscoplastic bounding surface model for cohesive soils. Soils and Foundations, 30(3):11–24.

Li, L. L. Dan, H. B. and Wang, L. Z. 2011. Undrained behavior of natural marine clay under cyclic loading, *Ocean Engineering*. 38(16): 1792–1805.

Martindale, H. Chakraborty, T. and Basu, B. A. 2013. strain-rate dependent clay constitutive model with parametric sensitivity and uncertainty quantification. Geotechnical and Geological Engineering, 31:229–48.

Martin, J. R., Olgun, C. G. Mitchell, J. K. and Durgunoglu, H. T. 2004. High-modulus columns for liquefaction mitigation. *Journal of geotechnical and geoenvironmental engineering*, ASCE, *130*(6), 561-571.

Ni, J. B. and Indraratna, X. Y. 2014. Model of soft soils under cyclic loading. *International Journal of Geomechanics*. 15 (4): 04014067.

Roscoe, K. H. and Burland, J. B. 1968. On the generalized stress-strain behaviour of wet clay. *Engineering plasticity, edited by J. Heyman and F. A. Leckie*, 535–609. Cambridge, UK: Cambridge University Press.

Seed, H. B. and Idriss, I. M. 1967. Analysis of soil liquefaction: *Niigata earthquake. Journal of the Soil Mechanics and Foundations Division*, 93(3), 83-108.

Shi, Z., Finno, R. J. and Buscarnera, G. 2018. A hybrid plastic flow rule for cyclically loaded clay, *Computers and Geotechnics*, 101: 65-79.

Shi, Z. Hambleton, J. P. and Buscarnera, G. 2019. Bounding Surface Elasto-Viscoplasticity: A General Constitutive Framework for Rate-Dependent Geomaterials. *Journal of Engineering Mechanics*, 145(3): 04019002.

Taiebat, M. Dafalias, Y. F. and Peek, R. 2010. A destructuration theory and its application to SANICLAY model*. International Journal for Numerical and Analytical Methods in Geomechanics*, 34(10): 1009-1040.

Yin, Z. Y. and Hicher, P. Y. 2008. Identifying parameters controlling soil delayed behavior from laboratory and in situ pressuremeter testing. *International Journal for Numerical and Analytical Methods in Geomechanics,* 32: 1515–35.